Cluster Catalysis

International Edition: DOI: 10.1002/anie.201903853
German Edition: DOI: 10.1002/ange.201903853

Reversible Switching of Catalytic Activity by Shuttling an Atom into and out of Gold Nanoclusters

Xiao Cai, Govindarajan Saranya, Kangqi Shen, Mingyang Chen, Rui Si,* Weiping Ding, and Yan Zhu**

Abstract: *It is challenging to control the catalyst activation and deactivation by removal and addition of only one central atom, as it is almost impossible to precisely abstract an atom from a conventional catalyst and analyze its catalysis. Here we report that the loss of one central atom in Au_{25} (resulting in Au_{24}) enhances the catalytic activity in the oxidation of methane compared to the original Au_{25}. More importantly, the activity can be readily switched through shuttling the central atom into Au_{24} and out of Au_{25}. This work will serve as a starting point for design rules on how to control catalytic performance of a catalyst by an atom alteration.*

Every atom of a catalyst can be directly or indirectly involved in a reaction process. However, it is difficult to distinguish the contribution of individual atom on different sites in a catalyst to the catalytic performance, as it is challenging to control the catalyst activation and deactivation by addition or removal of an atom. In the subnanometer size regime, every atom of a catalyst can have a potential influence on the overall performance,[1] and hence it is necessary to gain fundamental insights into catalysis of one atom on a special site. With the successful attainment of atomically precise metal nanoclusters capped by ligands,[2] where an atom of a nanocluster can be replaced by a foreign atom without altering the atomic structure of the nanocluster,[3] an opportunity for unravelling catalysis of one doping atom has been provided. For example, it has been reported that replacing the central atom of Au nanoclusters with a platinum atom caused a drastic increase in the catalytic activity for selective oxidation of styrene or the hydrogenation production.[4] The Au_{25} nanocluster doped by a Pd atom showed an enhancement in aerobic alcohol oxidation.[5] Our group found that the central doping of a foreign atom (Au, Pd or Pt) into the Ag_{25} nanocluster can have a substantial influence on the catalytic reactivity in the carboxylation reaction of CO_2 with terminal alkyne.[6] These studies indicate that the alteration of a catalyst by a foreign dopant that leads to a heterometal catalyst can drastically change the catalytic properties of the original catalyst. In particular, recent success in shuttling single gold atom into $[Au_{24}(PPh_3)_{10}(SC_2H_4Ph)_5Cl_2]^+$ (abbreviated as Au_{24}, hereafter) and out of $[Au_{25}(PPh_3)_{10}(SC_2H_4Ph)_5Cl_2]^{2+}$ (abbreviated as Au_{25}, hereafter)[7] allows us to explore how the catalytic properties of a homometal catalyst are dominated by addition or removal of a single metal atom.

Au_{24} and Au_{25} nanoclusters have identical surface atomic organization, as shown in Figure 1 a, which can be viewed as two vertex-sharing Au_{13} icosahedrons coordinated to five thiolate linkages; the top and bottom Au_5 pentagons are linked by ten triphenylphosphine; the two apex gold atoms are bound to two Cl atoms. It is noted that the only difference of Au_{24} and Au_{25} is that Au_{24} misses the central atom. Here we demonstrate that one-central-atom loss in the Au_{24} nanocluster enables better catalytic activity in the methane oxidation toward methanol compared to the Au_{25} nanocluster. More importantly, the activation and deactivation can be reversibly switched by losing the central atom and filling the central vacancy, which effectively avoids the irreversibility of catalytic capability and improves the durability.

The two gold nanoclusters were analyzed by electrospray ionization mass spectrometry (ESI-MS) and determined to be $Au_{24}(PPh_3)_{10}(SC_2H_4Ph)_5Cl_2$ and $Au_{25}(PPh_3)_{10}(SC_2H_4Ph)_5Cl_2$ (Figure 1 b). The UV-vis absorption spectrum of Au_{24} showed prominent peaks at 382 and 560 nm, while the absorption peaks in Au_{25} were located at 415 and 670 nm (Figure 1 c). X-ray photoelectron spectroscopy (XPS) studies showed that the Au 4f binding energies of Au_{24} were positively shifted, compared to Au_{25} (Figure S1 shown in Supporting Information). The presence of Au^0 and Au^+ was in the Au 4f spectra of the two nanoclusters, in which the Au^+ species appeared on the surface of nanoclusters, mainly owing to the electron donation occurring from the surface Au atoms to the ligands.[8] The mole ratio of Au^+ to Au^0 was 0.68 for Au_{24} and 0.52 for Au_{25}, respectively. The data suggest that Au_{24} carried more positive charge in comparison with Au_{25}.

The changes in the gold charge state were also monitored by X-ray absorption near edges structure (XANES) studies (Figure 1 d), which indicated that the average charge state of Au_{24} (+0.53) was more positive than that of Au_{25} (+0.35) by the aids of liner combination fits (Figure S2).[9] Furthermore, local coordination environments in Au_{24} and Au_{25} were probed by extended X-ray absorption fine structure

[*] X. Cai, Prof. W. Ding, Prof. Y. Zhu
Key Lab of Mesoscopic Chemistry, School of Chemistry and Chemical Engineering, Nanjing University
Nanjing 210093 (China)
E-mail: zhuyan@nju.edu.cn
G. Saranya, K. Shen, Prof. M. Chen
Beijing Computational Science Research Center
Beijing 100193 (China)
E-mail: mychen@csrc.ac.cn
Prof. R. Si
Shanghai Radiation Facility, Shanghai Institute of Applied Physics, Chinese Academy of Sciences
Shanghai 201204 (China)
E-mail: sirui@sinap.ac.cn
Supporting information and the ORCID identification number(s) for the author(s) of this article can be found under https://doi.org/10.1002/anie.201903853.

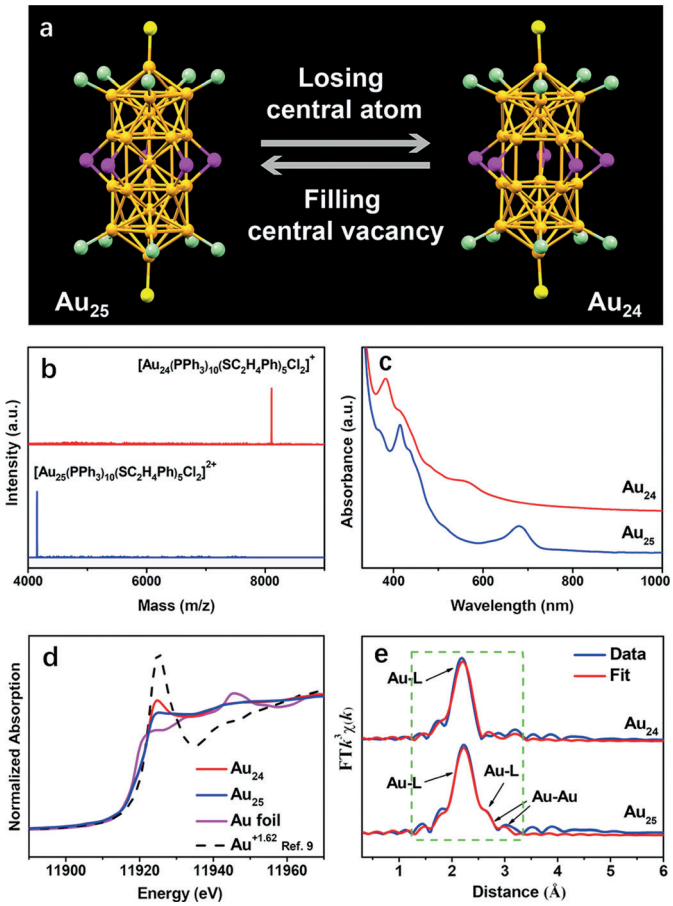

Figure 1. a) Atomic structures of Au_{24} with the central vacancy and Au_{25} with the central atom (Color label: Au, orange; S, pink; Cl, yellow; P, green. C and H atoms are omitted for clarity). b) ESI-MS spectra of Au_{24} and Au_{25}. c) UV-vis spectra of Au_{24} and Au_{25}. d) XANES and e) EXAFS profiles of Au_{24} and Au_{25}. (L = P/S; Green dash rectangle frame indicates the fitted R range.)

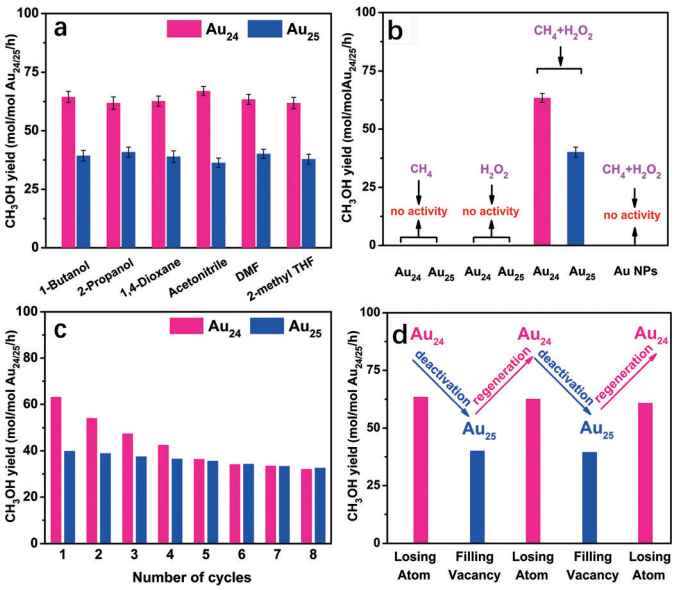

Figure 2. a) Catalytic performance of methane oxidation over the Au_{24} and Au_{25} catalysts in the different solvents. b) Comparison of catalytic properties of the gold catalysts under different reaction conditions. c) Recyclability of Au_{24} and Au_{25}. d) Activity reversible behavior of Au_{24} and Au_{25}. Reaction conditions: 1 mg gold, 0.3 M H_2O_2, 15 mL DMF, 2 MPa CH_4, 50 °C.

(EXAFS) experiments. Besides the capped ligands, as shown in Figure 1e, Au_{25} showed an extra Au-Au contribution (split peaks at ca. 2.75 Å, more details in Figure S2 and Table S1), uniquely originated from the center gold atom. Other gold-gold bonds in either Au_{24} or Au_{25} disappeared in EXAFS spectra, probably due to the thermal fluctuation of Au-Au bonds at room temperature.[10] Note that the Au-Au bonds in small Au clusters were visible only when the EXAFS data were collected at low temperature (8 K).[11]

One-central-atom loss in the Au_{24} nanocluster induced a significant perturbation to the electronic structure, which may render different catalytic properties. Therefore, catalysis of the Au_{24} and Au_{25} nanoclusters was explored, in which catalytic conversion of methane was used as a model reaction. As shown in Figure 2a, the Au_{24} catalyst was more effective than the Au_{25} catalyst for catalytic oxidation of methane with H_2O_2. Notably, both Au_{24} and Au_{25} nanoclusters efficiently converted methane to methanol. As presented in Figure 2b, typical Au nanoparticles manifested in Figure S3–4 had no catalytic activity under identical experimental conditions.

Considering that the ligand-capped Au_{24} and Au_{25} contained carbon sources, the comparison experiments were done. Either CH_4 or H_2O_2 was introduced and no product was detected (Figure 2b). ^{13}C nuclear magnetic resonance (NMR) studies further supported the product derived from methane and meanwhile confirmed the liquid product assigned to methanol (Figure S5). The results not only rule out methanol evolution from the Au's organic ligands, but also verify that the Au_{24} and Au_{25} catalysts can convert methane to methanol.

More interestingly, the performances of recycled catalysts gave us the new aspects about the reversible activity of the two nanoclusters in the reaction. Au_{24} was more active but less stable than Au_{25} and with cycles Au_{24} went through a continued slowdown in activity close to Au_{25} (Figure 2c). Our studies showed that the structure of Au_{24} appeared to be rearranged under the existence of H_2O_2. The evolution of the UV-vis spectra of the Au_{24} and Au_{25} in H_2O_2 not only showed that the atomicity of Au_{25} was rather preserved, but also revealed that Au_{24} underwent a structure transformation into Au_{25} (Figure S6), which was also supported by ESI-MS spectra (Figure S7). Notably, inspired by the last stage of Au_{24} synthesis, we envisioned a structure regeneration of Au_{24} by the destroyed Au_{24} (in fact it had been Au_{25}) reacting with the excess PPh_3. As expected, the conversion between Au_{24} and Au_{25} was completely reversible: Au_{25} was converted back to Au_{24} (Figure S8) and the activity was recovered (Figure 2d). The phenomena clearly indicate that the activity is readily switchable through shuttling the central atom into Au_{24} and out of Au_{25}. The reversible activity is of particular importance to avoid the irreversible inactivation and the fading of cycle life.

To understand catalysis of one-central-atom removal and addition, the reaction mechanism of methane oxidation catalyzed by the Au_{24} and Au_{25} catalysts was investigated in

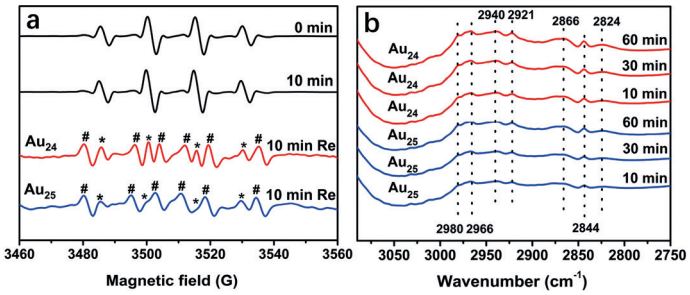

Figure 3. a) EPR spectra of CH_4 reaction with H_2O_2: spectra obtained from H_2O_2 solution before the introduction of CH_4 (0 min); after 10 min reaction of CH_4 and H_2O_2 without the catalyst; after 10 min reactions of CH_4 and H_2O_2 catalyzed by Au_{24} and Au_{25}. b) ATR-IR spectra of CH_4 reaction with H_2O_2 catalyzed by Au_{24} and Au_{25}.

detail. Firstly the potential radical species were detected by electron paramagnetic resonance spectroscopy (EPR) with 5,5-dimethylpyrroline-*N*-oxide (DMPO) as a radical trapping agent. As shown in Figure 3a, before the introduction of methane, a characteristic signal (1:2:2:1) corresponding to DMPO-OH adduct was found, revealing the presence of hydroxyl radicals. After the introduction of methane and H_2O_2 in the system for 10 min, only ·OH adduct with DMPO was observed. When the gold clusters were added to the system containing methane and H_2O_2, besides ·OH adduct (asterisk symbol), ·CH_3 adduct (well symbol) with DMPO was also detected (Figure 3a). Further, the addition of the hydroxyl radical scavenger (Na_2SO_3) into the reactions led to the decrease of methane conversion (Figure S9). It indicates that hydroxyl radicals are the major active oxygen species.

To determine the potential intermediate species adsorbed over the Au_{24} and Au_{25} catalysts in the oxidation of methane, attenuated total reflection infrared (ATR-IR) spectra were performed by exposure of the two nanoclusters to methane and H_2O_2. From Figure 3b, the two bands were visible at 2966 and 2921 cm^{-1}, which are assigned to the asymmetric C–H stretching vibrations of methoxy groups.[12] The band at 2940 cm^{-1} is assigned to an overtone deformation vibration of methoxy groups and the band at 2824 cm^{-1} is associated with a symmetric C–H stretching vibration of methoxy groups.[13] The bands at 2980 and 2866 cm^{-1} can be assigned to asymmetric and symmetric C–H stretches of methoxy groups produced by the reaction of methanol with hydroxyl groups, respectively.[14] The ν_s(C–H) mode of OCH_3 groups appearing at 2844 cm^{-1} was also detected.[15] The results imply that the reactions of methane with H_2O_2 over the two nanoclusters are accompanied with the formation of methoxy species.

Furthermore, the reaction pathways and energy profiles for the methane oxidation over Au_{24} and Au_{25} were explored by Density functional theory (DFT) calculations. Initially, a H_2O_2 dissociatively adsorbs as two ·OH at two surface Au sites. All the surface Au atoms except the two apex Au atoms bonded to Cl can adsorb OH exothermically ($E_{ads} \approx -30$ kcal mol^{-1}). The adsorbed OH on the intact catalyst cannot initiate CH_4 activation. Instead, OH at open Au of the partial cleavage of the Au-thiol-Au bridge can react with CH_4 (**25b** and **24b** in Figure 4a and c; the optimized geometries in Figure S10), with E_{ads}(OH) ≈ 20 kcal mol^{-1}. The reaction pathway for the less reactive Au_{25} was first considered (Figure 4a and 4b). CH_4 is activated via a triangular transition state (TS) **25d**, with the barrier height $\Delta H^{\ddagger} \approx 30$ kcal mol^{-1}, leading to **25e**. The partial cleavage exposes a low-coordination surface Au and provides enough reaction space around the singly adsorbed Au-OH to activate CH_4 and accept ·CH_3 from CH_4 activation. Alternatively, if two OH are adsorbed at the partial cleavage (**25c**), the CH_4 activation is suppressed. For CH_3 and OH to recombine in **25e**, OH must migrate to adjacent Au that adsorbs CH_3, as the orientation of HO-Au1-Au2-CH_3 forbids the two-site recombination (∡Au1-Au2-C = 125°). The OH migration can be done via bending ∡Au2-Au1-O, leading to **25f**. A rigid scan of ∡Au2-Au1-O shows the migration requires > 40 kcal mol^{-1} to overcome the barrier (Figure S11a). The successive one-site recombination of CH_3 and OH (**25f** → **25h** via **TS 25g**) has a low barrier of ≈15 kcal mol^{-1}. The so-formed CH_3OH in **25h** is weakly adsorbed ($E_{ads} \approx 5$ kcal mol^{-1}).

The reaction with Au_{24} could take a pathway similar to the Au_{25} pathway, with exactly alike energetics (black paths in Figure 4c and d). If so, Au_{24} and Au_{25} would exhibit similar catalytic behaviors, which contradicts the experimental results. DFT reveals that the central vacancy enables two additional shortcut pathways (red and blue paths in Figure 4c and d) that can enhance catalysis of Au_{24}. A surface Au can facilely migrate to fill the vacancy at the rod center (Figure S12) with $\Delta H^{\ddagger} = 9$ kcal mol^{-1}. The resulting Au_{24} complexes are denoted as M-Au_{24} complexes and are indicated by * in their labels. Both shortcut pathways avoid the rate-limiting OH migration barrier along **24e** → **24f**. The first shortcut connects **24a** and **24f**, along which the one-site CH_4 activation (**24b** → **24e**) and succeeding OH migration are replaced by a two-site reaction (**24b*** → **24f** via **TS 24d*** with $\Delta H^{\ddagger} = 30$ kcal mol^{-1}). The second shortcut deviates from **24e** and terminates at **24h**, where the one-site CH_3-OH recombination (**24f** → **24h**) and preceding OH migration are replaced by a two-site CH_3-OH recombination (**24e*** → **24h** via **TS 24g*** with $\Delta H^{\ddagger} = 27$ kcal mol^{-1}) that directly leads to the CH_3OH product (**24h**). The two-site reactions are enabled by suitable Au-adsorbate orientations at the central site of M-Au_{24}. For example, in **24e***, ∡Au1-Au2-C of the HO-Au1-Au2-CH_3 site is 86°, so bending ∡Au2-Au1-O directly leads to TS of two-site recombination reaction (Figure S11b). Conversely, bending ∡Au2-Au1-O in **24e** and **25e** only leads to a pre-recombination intermediates.

In addition, the isomerization from Au_{24} to M-Au_{24} also increases the mobility of OH adsorbate, and enhances CH_3-OH recombination. For Au_{25}, the trajectory of OH connects two surface Au atoms on the Au_5 pentagon ring of the icosahedral Au_{12} sphere and is always under substantial steric effect of Au-PPh_3, indicated by the barrier at ∡Au-Au-OH ≈ 90° during the **25e** → **25f** rigid scan (Figure S11a). For M-Au_{24} **24e*** → **24g*** transition, the trajectory of OH connects a surface Au and the central Au, and the steric effect on OH decreases as OH moves towards the central Au.

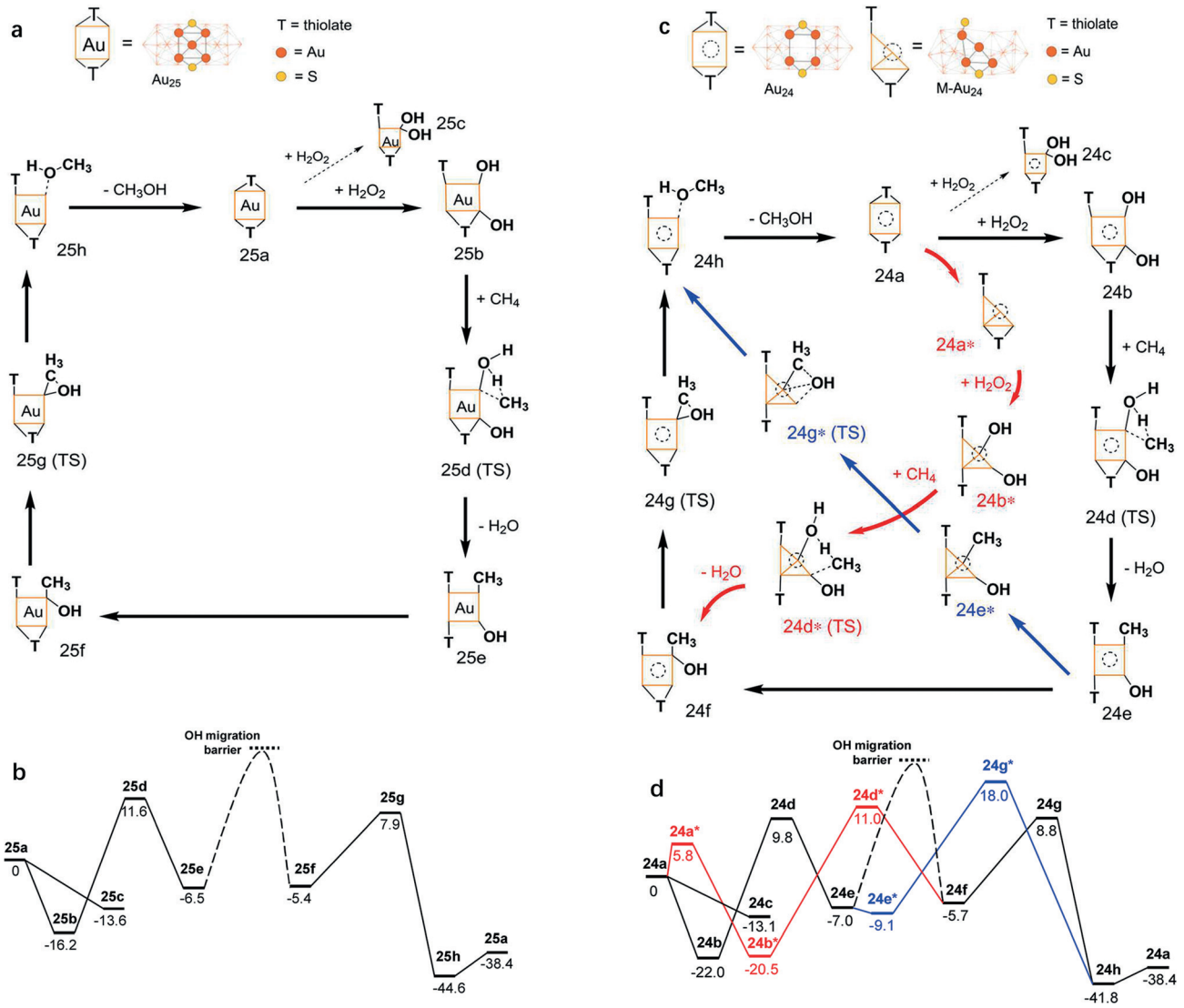

Figure 4. Proposed catalytic mechanism and predicted reaction enthalpy profiles for the methane oxidation on a, b) Au_{25} and c, d) Au_{24} at the DFT PBE/LANL2DZ level with $[Au_{24/25}(PH_3)_8(PPh_3)_2(SCH_3)_2(SC_2H_4Ph)_3Cl_2]^{+/2+}$ models using GAUSSIAN09 program. Reaction enthalpies are at 0 K in kcal mol^{-1}. Au_{24} and Au_{25} complexes are labeled as 24N and 25N, **N** = **a**, **b**, **c**, etc., and M-Au_{24} complexes are denoted as 24N*. All of the corresponding optimized geometries can be found in Figure S10. Black paths indicate the reaction pathways for Au_{25} and Au_{24} without involving the central vacancy, whereas the red and blue paths indicate the shortcut-pathways that involve M-Au_{24}.

In brief, DFT calculations show that the methane to methanol conversion on the Au_{24} and Au_{25} catalysts are facilitated by the heterogenous active sites on the surface of the nanoclusters. The PPh_3 and SC_2H_4Ph protected Au sites can adsorb free $^{\bullet}OH$ in the reaction. The partial cleaved bridge Au sites induced by OH insertion can promote CH_4 activation, and adsorb the resulting CH_3. The M-Au_{24} isomer of Au_{24}, resulting from the migration of the central vacancy in Au_{24}, enables the two-site reaction steps that enhance catalysis of Au_{24}, which can be insightful in designing catalytic reactions that involve two small fragments. More supplemental discussion about the structural and electronic properties of Au_{24} and Au_{25} at DFT level, geometry optimizations for intermediates, and transition states can be found in Supporting Information.

In summary, our studies show that the alteration of a gold nanocluster by one central atom can significantly change the catalytic properties. The catalytic activity can be switched by one-central-atom removal and addition. The work impacts our understanding of the contributions of individual atoms on different sites in a catalyst to the catalytic performance and provides design rules on how to control the catalytic properties of a catalyst by one-atom removal and addition.

Acknowledgements

We acknowledge financial support from National Natural Science Foundation of China (21773109, 91845104, and U1530401) and Fundamental Research Funds for the Central

Universities. We thank Prof. Rongchao Jin from Carnegie Mellon University for helpful discussion.

Conflict of interest

The authors declare no conflict of interest.

Keywords: cluster catalysis · gold nanoclusters · methane oxidation

How to cite: *Angew. Chem. Int. Ed.* **2019**, *58*, 9964 – 9968
Angew. Chem. **2019**, *131*, 10069 – 10073

[1] M. M. Shoshani, S. A. Johnson, *Nat. Chem.* **2017**, *9*, 1282 – 1285.
[2] a) P. D. Jadzinsky, G. Calero, C. J. Ackerson, D. A. Bushnell, R. D. Kornberg, *Science* **2007**, *318*, 430 – 433; b) A. Desireddy, B. E. Conn, J. Guo, B. Yoon, R. N. Barnett, B. M. Monahan, K. Kirschbaum, W. P. Griffith, R. L. Whetten, U. Landman, T. P. Bigioni, *Nature* **2013**, *501*, 399 – 402; c) M. Azubel, J. Koivisto, S. Malola, D. Bushnell, G. L. Hura, A. L. Koh, H. Tsunoyama, T. Tsukuda, M. Pettersson, H. Häkkinen, R. D. Kornberg, *Science* **2014**, *345*, 909 – 912; d) C. Zeng, Y. Chen, K. Kirschbaum, K. J. Lambright, R. Jin, *Science* **2016**, *354*, 1580 – 1584; e) Q. Yao, V. Fung, C. Sun, S. Huang, T. Chen, D. Jiang, J. Y. Lee, J. Xie, *Nat. Commun.* **2018**, *9*, 1979; f) X. Wan, Z. Guan, Q. Wang, *Angew. Chem. Int. Ed.* **2017**, *56*, 11494 – 11497; *Angew. Chem.* **2017**, *129*, 11652 – 11655.
[3] a) M. S. Bootharaju, C. P. Joshi, M. R. Parida, O. F. Mohammed, O. M. Bakr, *Angew. Chem. Int. Ed.* **2016**, *55*, 922 – 926; *Angew. Chem.* **2016**, *128*, 934 – 938; b) C. Yao, Y. Lin, J. Yuan, L. Liao, M. Zhu, L. Weng, J. Yang, Z. Wu, *J. Am. Chem. Soc.* **2015**, *137*, 15350 – 15353; c) Y. Negishi, W. Kurashige, Y. Kobayashi, S. Yamazoe, N. Kojima, M. Seto, T. Tsukuda, *J. Phys. Chem. Lett.* **2013**, *4*, 3579 – 3583; d) J. Yan, H. Su, H. Yang, S. Malola, S. Lin, H. Hakkinen, N. Zheng, *J. Am. Chem. Soc.* **2015**, *137*, 11880 – 11883.
[4] a) H. Qian, D. Jiang, G. Li, C. Gayathri, A. Das, R. R. Gil, R. Jin, *J. Am. Chem. Soc.* **2012**, *134*, 16159 – 16162; b) K. Kwak, W. Choi, Q. Tang, M. Kim, Y. Lee, D. Jiang, D. Lee, *Nat. Commun.* **2017**, *8*, 14723.
[5] S. Xie, H. Tsunoyama, W. Kurashige, Y. Negishi, T. Tsukuda, *ACS Catal.* **2012**, *2*, 1519 – 1523.
[6] Y. Liu, X. Chai, X. Cai, M. Chen, R. Jin, W. Ding, Y. Zhu, *Angew. Chem. Int. Ed.* **2018**, *57*, 9775 – 9779; *Angew. Chem.* **2018**, *130*, 9923 – 9927.
[7] S. Wang, H. Abroshan, C. Liu, T. Luo, M. Zhu, H. J. Kim, N. L. Rosi, R. Jin, *Nat. Commun.* **2017**, *8*, 848.
[8] Y. Negishi, K. Nobusada, T. Tsukuda, *J. Am. Chem. Soc.* **2005**, *127*, 5261 – 5270.
[9] L. Guo, P. Du, X. Fu, C. Ma, J. Zeng, R. Si, Y. Huang, C. Jia, Y. Zhang, C. Yan, *Nat. Commun.* **2016**, *7*, 13481.
[10] P. Zhang, *J. Phys. Chem. C* **2014**, *118*, 25291 – 25299.
[11] S. Yamazoe, S. Takano, W. Kurashige, T. Yokoyama, K. Nitta, Y. Negishi, T. Tsukuda, *Nat. Commun.* **2016**, *7*, 10414.
[12] B. R. Wood, J. A. Reimer, A. T. Bell, M. T. Janicke, K. C. Ott, *J. Catal.* **2004**, *225*, 300 – 306.
[13] S. Kameoka, T. Nobukawa, S. I. Tanaka, S. I. Ito, K. Tomishige, K. Kunimori, *Phys. Chem. Chem. Phys.* **2003**, *5*, 3328 – 3333.
[14] S. M. Campbell, X. Jiang, R. F. Howe, *Microporous Mater.* **1999**, *29*, 91 – 108.
[15] R. Tumma, S. Siliveri, H. B. Vamaraju, M. R. Bommineni, *J. Pharm. Res.* **2017**, *11*, 895 – 902.

Manuscript received: March 29, 2019
Revised manuscript received: April 30, 2019
Accepted manuscript online: May 20, 2019
Version of record online: June 11, 2019

